Extended Curtin-Hammett principle: Origin of pathway selection in reversible reaction networks under kinetic control

Satoshi Takahashi,[1] Hirofumi Sato,[2,3] and Shuichi Hiraoka[1,*]

[1]Department of Basic Science, Graduate School of Arts and Sciences, The University of Tokyo, Tokyo 153-8902, Japan.

[2]Department of Molecular Engineering, Kyoto University, Kyoto 615-8510, Japan

[3]Fukui Institute for Fundamental Chemistry, Kyoto University, Kyoto 606-8103, Japan

*Correspondence: hiraoka-s@g.ecc.u-tokyo.ac.jp

Abstract

Curtin-Hammett principle works in a reaction sequence where slow irreversible reactions are connected to a fast reversible reaction and determines the product distribution depending only on the relative energy barriers of the two irreversible reactions, resulting in kinetic pathway selection. A basic question is whether Curtin-Hammett principle is applicable to reaction networks composed of reversible elementary reactions, though reversible reactions are generally governed by the laws of thermodynamics. Numerical simulations of model systems where reversible elementary reactions are connected linearly to an initial reversible reaction demonstrate that a metastable state far from equilibrium is transiently produced and that its lifetime is prolonged with increasing the number of connected reversible reactions. Pathway selection based on this extended concept of Curtin-Hammett principle was observed in molecular self-assembly of a Pd_6L_4 truncated tetrahedron, which supports the idea that the extended Curtin-Hammett principle is a key general concept underlining kinetic control in reversible reaction networks.

Introduction

Chemical reaction network is the key concept in the origin of functions in living systems, such as regulation[1-3], amplification[4,5], oscillation[6-10], transduction[11-13], signaling[14-17], photosynthesis[18-21], and metabolism[22-28]. Although kinetics of the elementary reactions in the network are very simple, unexpected results like emergence are sometimes observed due to mutual correlation among the reactions. Such emergent behaviors have been analyzed and understood by mathematical models,[29-33] which enable us to abstract universality in similar and related phenomena.[34-36] Most of above-mentioned systems are composed of irreversible reactions, so the direction of each elementary reaction is basically determined. In contrast, it is generally considered that reversible chemical reactions finally reach thermodynamic equilibrium, so the kinetics in reaction networks composed of reversible elementary reactions have been underestimated. However, such reversible reaction networks sometimes lead to metastable, kinetic states as seen in protein folding[37,38] and self-assembly[39-41]. Most of these metastable states are kinetic traps with relatively high kinetic stability and should be selectively produced by pathway selection in the reaction network. Reaction networks composed of reversible elementary reactions are highly adaptive because even the direction of each elementary reaction is affected by other reversible elementary reactions, which is different from irreversible reaction networks. So, understanding of kinetic behavior of reversible reaction networks is complicated and the general principle of pathway selection in reversible reaction networks has not been established yet.

The well-known Curtin-Hammett (C-H) principle[42-46] is a good starting point to consider how the reaction proceeds kinetically in the network containing reversible reaction(s). The simplest reaction network model considered in the C-H principle is shown in Fig. 1, where slow irreversible reactions (**A** $\xrightarrow{k_{AC}}$ **C** and **B** $\xrightarrow{k_{BD}}$ **D**) are connected to a fast reversible reaction (**A** ⇄ **B**). The ratio of the final products (**C** and **D**) is not solely determined by the relative proportions of substrates (**A** and **B**), $K_{AB} \equiv k_{AB}/k_{BA}$, yet controlled by the difference in the energy barriers of the two irreversible reactions (k_{AC} and k_{BD}). This means that the fate of the reaction is dictated in a kinetically controlled manner. A question arises here: Is there a pathway selection principle like the C-H principle for reaction networks composed of reversible reactions?

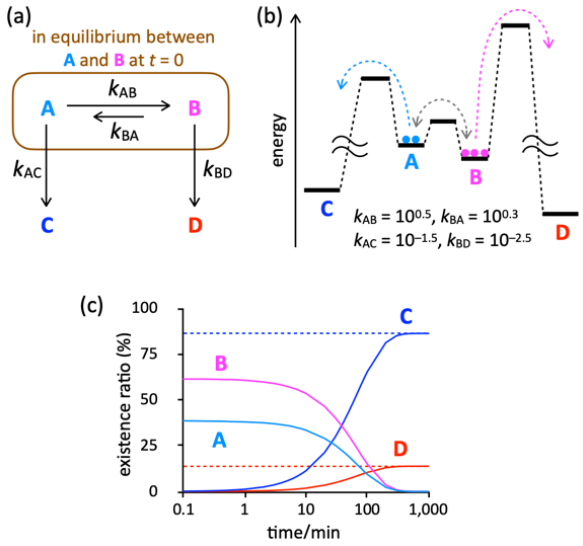

Figure 1. The simplest case of Curtin-Hammett principle. (a) A reaction network consisting of one reversible reaction (**A** ⇄ **B**) with two irreversible reactions (**B** → **D** and **A** → **C**). (b) A schematic energy diagram with the corresponding reaction rate constants in the reaction network model shown in (a). (c) The time evolution of existence ratios of the substrates (**A** and **B**) and the products (**C** and **D**) obtained by simulation with the initial concentrations given as those in equilibrium between the substrates **A** and **B**. Blue and red dashed lines indicate the product ratios in the Curtin-Hammett limit of the global reaction, where the product ratio ([**C**]/[**D**]) after the convergence is calculated as [**C**]/[**D**] = (k_{AB} × k_{BD})/(k_{AC} × k_{BA}) = ($10^{-1.5}$ min^{-1} × $10^{0.3}$ min^{-1})/($10^{0.5}$ min^{-1} × $10^{-2.5}$ min^{-1}) = $10^{0.8}$ = 6.3.

Here we show that the C-H principle can be extended in reaction networks composed of reversible reactions by numerical simulations with simple mathematical models. It was also found that (i) a transient kinetic state is generated even in the network whose elementary reactions are all reversible, and (ii) the lifetime of the transient state far from equilibrium is prolonged by increasing the number of connected reversible reactions. Then, we found that extended C-H principle is practically working in the essential part of pathway selection in the self-assembly of an M_6L_4 coordination cage composed of metal ion M and tritopic ligand L by the emergence of quasi-irreversibility in the network.

Results and Discussion

Appearance of pathway selection behavior in simple reaction networks consisting of reversible elementary reactions

Starting from the simplest C-H system shown in Fig. 1, three cases of reaction network models were established (Fig. 2). In these models, all the elementary reactions are treated as first-order for simplicity of discussion. In all the numerical simulations the time evolution was traced with the so-called Gillespie algorithm based on the chemical master equation[47-50] (see more detail in the Supporting Information).

Case 1: In case 1 (Fig. 2a), the irreversible **A** $\xrightarrow{k_{AC}}$ **C** reaction is as fast as **A** $\xrightarrow{k_{AB}}$ **B** in the reversible reaction (**A** ⇄ **B**), $k_{AC} = k_{AB}$, while $k_{AC} < k_{AB}$ in the original C-H model in Fig. 1. It was found that lowering the energy barriers of the irreversible reactions makes very little change of the global C-H behavior (Figs. 1c and 2a); Less stable **C** is produced over **D** in a similar yield of the original C-H case (blue broken line in Fig. 2a). This indicates that the C-H principle is valid even when the energy barriers between **A** and **B** are similar to that of **A** → **C** ($k_{AC} \simeq k_{AB}$ and k_{BA}). In other words, the irreversibility of the connected reactions (**A** → **C** and **B** → **D**) is the key of the C-H principle.

Case 2: Next, all the reactions in Case 1 are set to be reversible with the rate constants for the backward reactions, $k_{CA} = 10^{-1.5}$ min^{-1} and $k_{DB} = 10^{-2.5}$ min^{-1}. Note that for both **A** ⇄ **C** and **B** ⇄ **D** reactions the backward rate constants are given as 100 times lower than those for

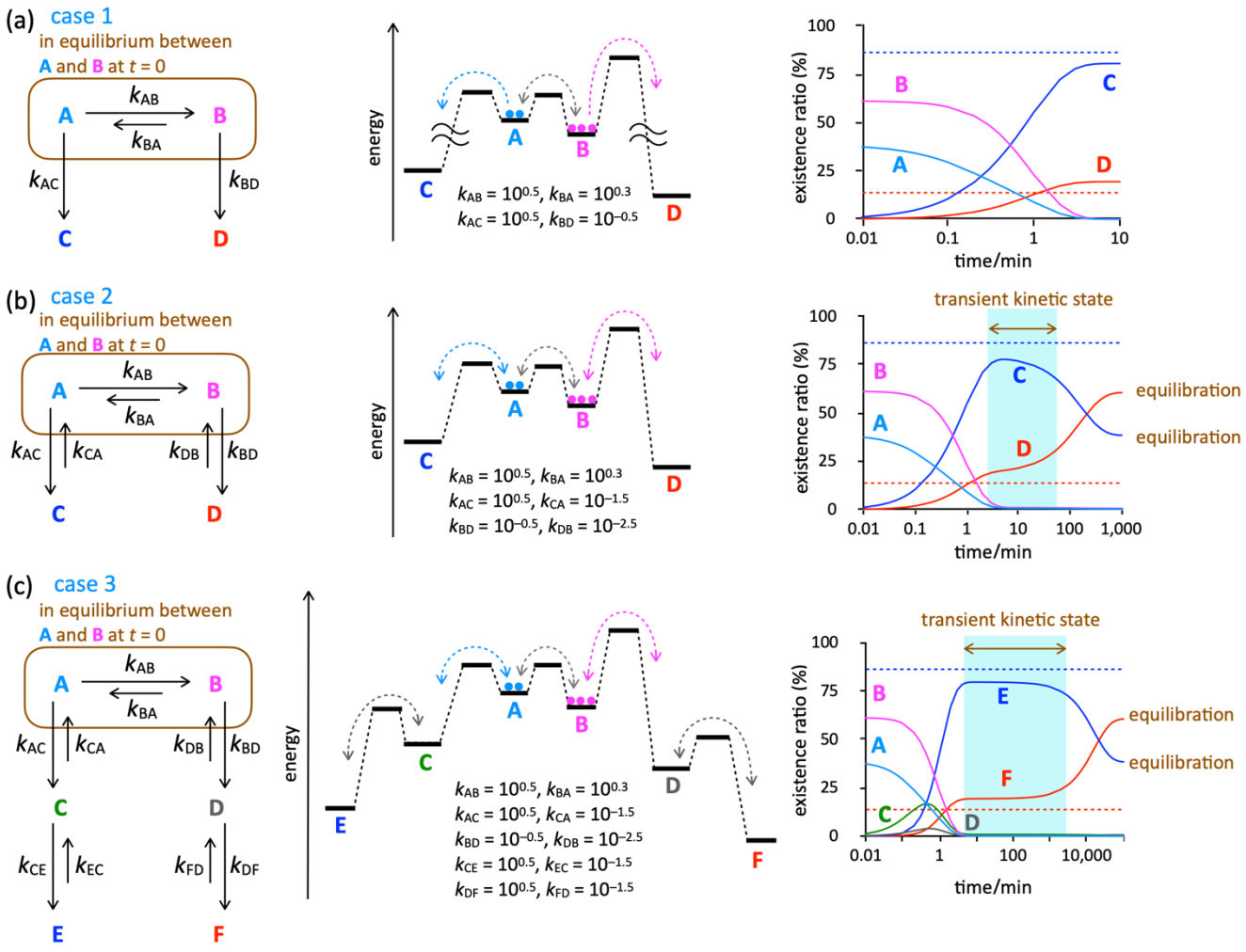

Figure 2. Mathematical models to verify extended concept of Curtin-Hammett (C-H) principle working in reaction networks consisting of reversible elementary reactions. (a) Check of the validity range of the C-H principle. The difference from the original C-H system in Fig. 1 is that the energy barrier of **A** → **C** is the same as that of **A** → **B** ($k_{AC} = k_{AB}$). (b) All the three elementary reactions are made reversible. A kinetic state is found to hold with a finite lifetime (a cyan rectangle). The product ratio [**C**]/[**D**] in equilibrium is calculated to be [**C**]/[**D**] = ($k_{AC} \times k_{BA} \times k_{DB}$)/($k_{BD} \times k_{AB} \times k_{CA}$) = $10^{(0.5+0.3-2.5)-(-0.5+0.5-1.5)}$ = 0.63. The transient kinetic state generated by the extended C-H principle is indicated by a cyan rectangle. (c) A reaction network composed of five reversible reactions where two reversible reactions (**C** ⇄ **E** and **D** ⇄ **F**) are connected to **C** and **D** in Case 2. Pathway selection to generate a transient kinetic state is realized. Lifetime of the kinetic state shown by a cyan rectangle is prolonged by increasing the number of the reversible reactions, with keeping a product ratio ([**E**]/[**F**]) calculated from the C-H principle. Blue and red broken lines indicate the existence ratios of the final products ([**C**] and [**D**] in Case 2, [**E**] and [**F**] in Case 3) in the reaction networks where the elementary reactions except **A** ⇄ **B** are irreversible ($k_{CA} = k_{DB} = k_{EC} = k_{FD} = 0$).

the forward ones (Fig. 2b). When the system finally reaches the thermodynamic equilibrium, **D** should be produced more than **C** because the thermodynamic stability of **D** is higher than that of **C**. In numerical simulation, the system reaches the equilibrium state in about 10 h with [**D**]>[**C**]. What is interesting is that the situation of [**C**]>[**D**] is transiently generated and the ratio of [**C**]/[**D**] is similar to that under the C-H condition (cyan-colored region in Fig. 2b). This result indicates that the C-H principle works even in a simple reaction network consisting of reversible elementary reactions to generate a transient kinetic state before reaching the global equilibration.

Case 3: Encouraged by the result in Case 2, we wonder if the transiently produced kinetic state governed by the C-H principle can be prolonged by connecting reversible reactions in both terminals in Case 2 (Fig. 2c). Two reversible reactions, **C** ⇄ **E** and **D** ⇄ **F**, whose rate constants are the same as that of **A** ⇄ **C**, are connected to **C** and **D** to make a reaction network composed of five reversible reactions. A striking feature found by this manipulation is significant extension of the transient kinetic state lifetime (for about 1.5 days!).

These results indicate that pathway selection to lead to a metastable, kinetic state is realized even in the reaction network where the elementary reactions are *all reversible* by the extended Curtin-Hammett principle and that the lifetime of such a transient kinetic state is prolonged by increasing the number of reversible elementary reactions. It should be noted that the transient kinetic state is generated due to emergence of the quasi-irreversibility of reaction(s) not to high kinetic stability of the metastable state.

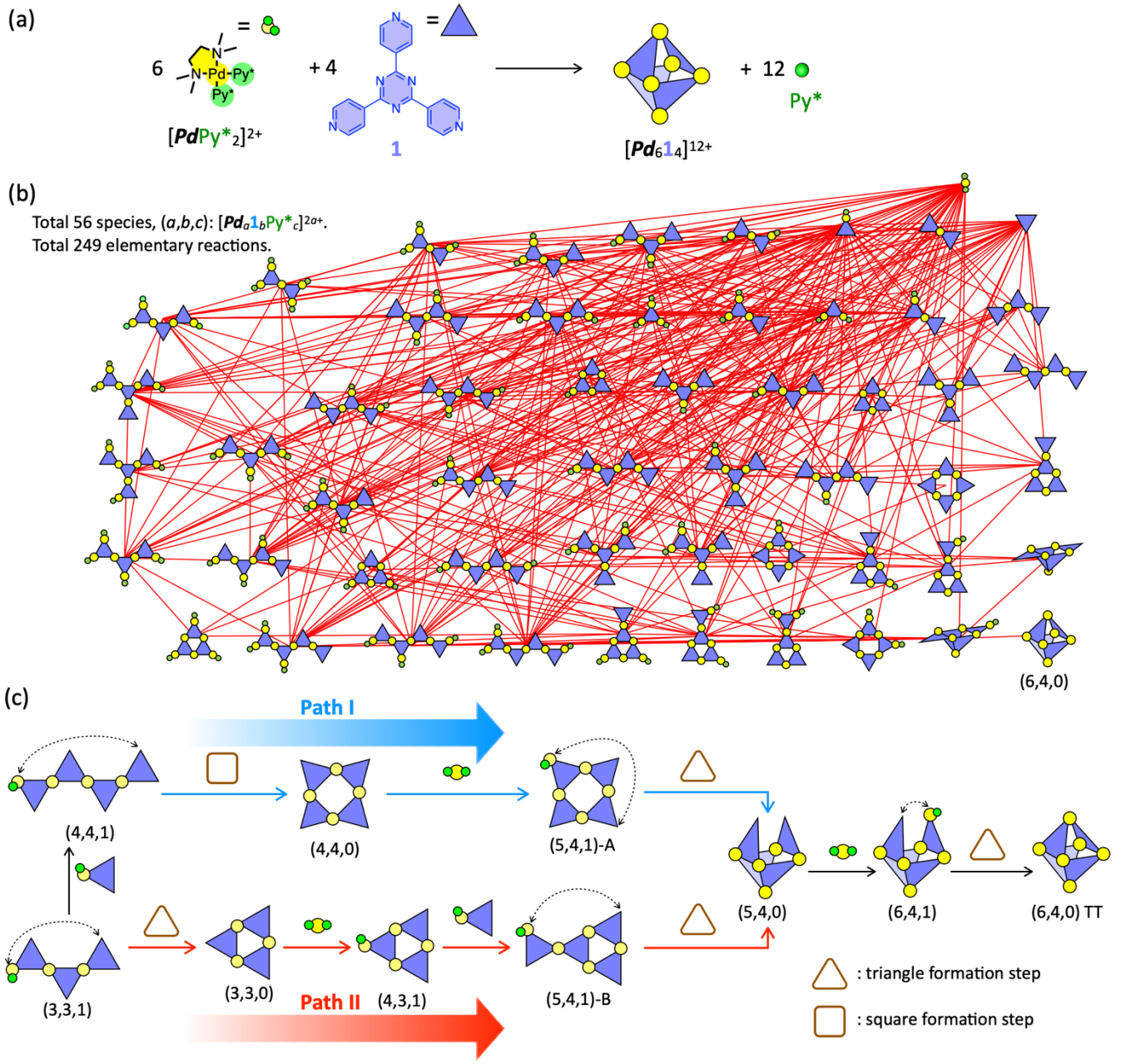

Figure 3. Self-assembly of a $[\mathbf{Pd_6 1_4}]^{12+}$ truncated tetrahedron (TT) from *cis*-protected Pd(II) complex and tritopic ligand **1**. (a) A schematic representation of the self-assembly of a $[\mathbf{Pd_6 1_4}]^{12+}$ TT. Py* indicates 3-chloropyridine. (b) A reaction network model established for the numerical analysis, where total 56 species and their total 249 elementary reactions are considered. Red lines indicate elementary reactions. (c) Two self-assembly pathways to the $[\mathbf{Pd_6 1_4}]^{12+}$ TT with different sequence of three intramolecular steps. Path **I** with blue arrows indicates a square → triangle → triangle sequence to form the $[\mathbf{Pd_6 1_4}]^{12+}$ TT, while path **II** with red arrows indicates that the $[\mathbf{Pd_6 1_4}]^{12+}$ TT is formed via a triangle → triangle → triangle sequence. (*a*,*b*,*c*) indicates $[\mathbf{Pd_a 1_b}\text{Py*}_c]^{2a+}$.

Pathway selection in molecular self-assembly of Pd_6L_4 cage

To see whether the pathway selection by the extended C-H principle is achieved in a more realistic system, the self-assembly process of a $[\mathbf{Pd}_6\mathbf{1}_4]^{12+}$ truncated tetrahedron (TT)[51] was analyzed. For this system, the possible self-assembly pathways can be classified into the following typical two groups based on the sequence of two kinds of cyclizations, i.e., triangle and square formations (Fig. 3c): (path **I**) square → triangle → triangle, and (path **II**) triangle → triangle → triangle, so the self-assembly of the $[\mathbf{Pd}_6\mathbf{1}_4]^{12+}$ TT is an appropriate system to discuss the pathway selection, though the final product is the same unlike the model systems in Fig. 2

The self-assembly of the $[\mathbf{Pd}_6\mathbf{1}_4]^{12+}$ TT was carried out by mixing *cis*-protected Pd(II) complex $[\mathbf{Pd}Py^*_2]^{2+}$ (***Pd***: Pd(TMEDA), Py*: 3-chloropyridine) and tritopic ligand **1**.[61] The time-course of the substrates ($[\mathbf{Pd}Py^*_2]^{2+}$ and **1**) and the products ($[\mathbf{Pd}_6\mathbf{1}_4]^{12+}$ and Py*) were monitored by ^{1}H NMR spectroscopy and the information about the intermediates derived from average composition of all intermediates, *n*-*k* values, were also obtained by QASAP (quantitative analysis of self-assembly process[52-57,60-63]) (Fig. 4a and b). The species in the self-assembly can be generally expressed as $[\mathbf{Pd}_a\mathbf{1}_b Py^*_c]^{2a+}$, where *a*-*c* indicate the number of components. $[\mathbf{Pd}_a\mathbf{1}_b Py^*_c]^{2a+}$ is denoted as (*a*,*b*,*c*) for simplicity. Average composition of all intermediates at time *t*, which can be obtained by experiment, is indicated as $[\mathbf{Pd}_{\langle a\rangle}\mathbf{1}_{\langle b\rangle}Py^*_{\langle c\rangle}]_t$. The intermediates are identified by two parameters, *n* and *k*, which are defined as $n = (2a - c)/b$ and $k = a/b$. The *n* value indicates the average number of ***Pd*** bound in a single tritopic ligand **1**. The *k* value indicates the ratio of ***Pd*** against **1**.

The experimental data thus obtained were numerically analyzed by NASAP (numerical analysis of self-assembly process)[58-63]. A reaction network model shown in Fig. 3b was established and the search of the reaction rate constants, which are classified into 7 types shown in Fig. 4c, in the network giving good fittings of the numerical results to the experimental counterparts (Fig. 4a and b).

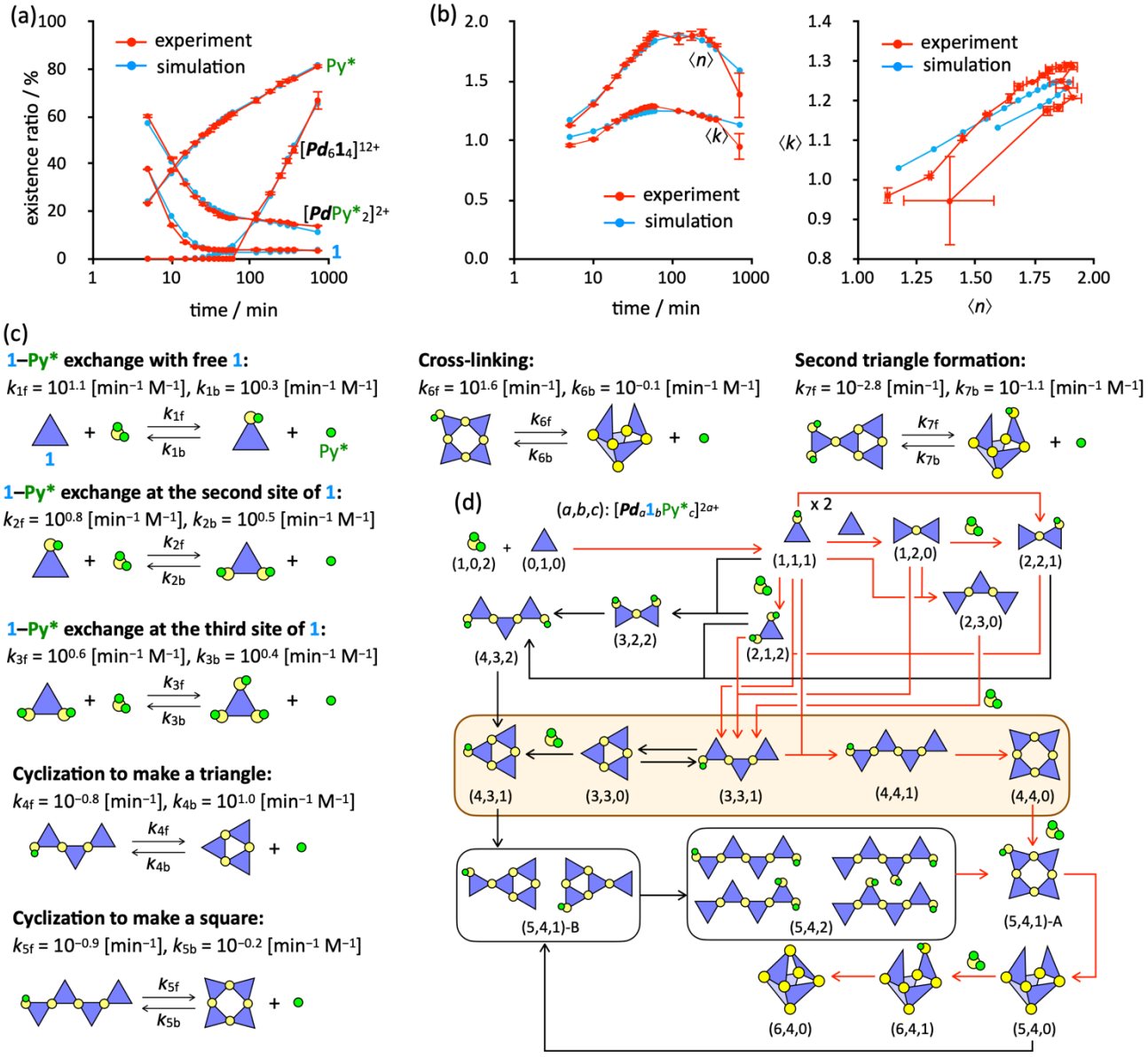

Figure 4. Quantitative analysis of the self-assembly process of the $[\mathbf{Pd}_6\mathbf{1}_4]^{12+}$ truncated tetrahedron (TT). (a) Existence ratios of the substrates and products with time. (b) Changes in the ⟨*n*⟩ and ⟨*k*⟩ values with time. The definition of the *n* and *k* values is indicated in the main text. (c) 7 types of elementary reactions classified in NASAP and their rate constants determined by numerical fitting to the experimental data in (a) and (b). (d) Dominant self-assembly pathways determined by numerical simulation with the fixed rate constants. The major self-assembly pathways are indicated by red arrows.

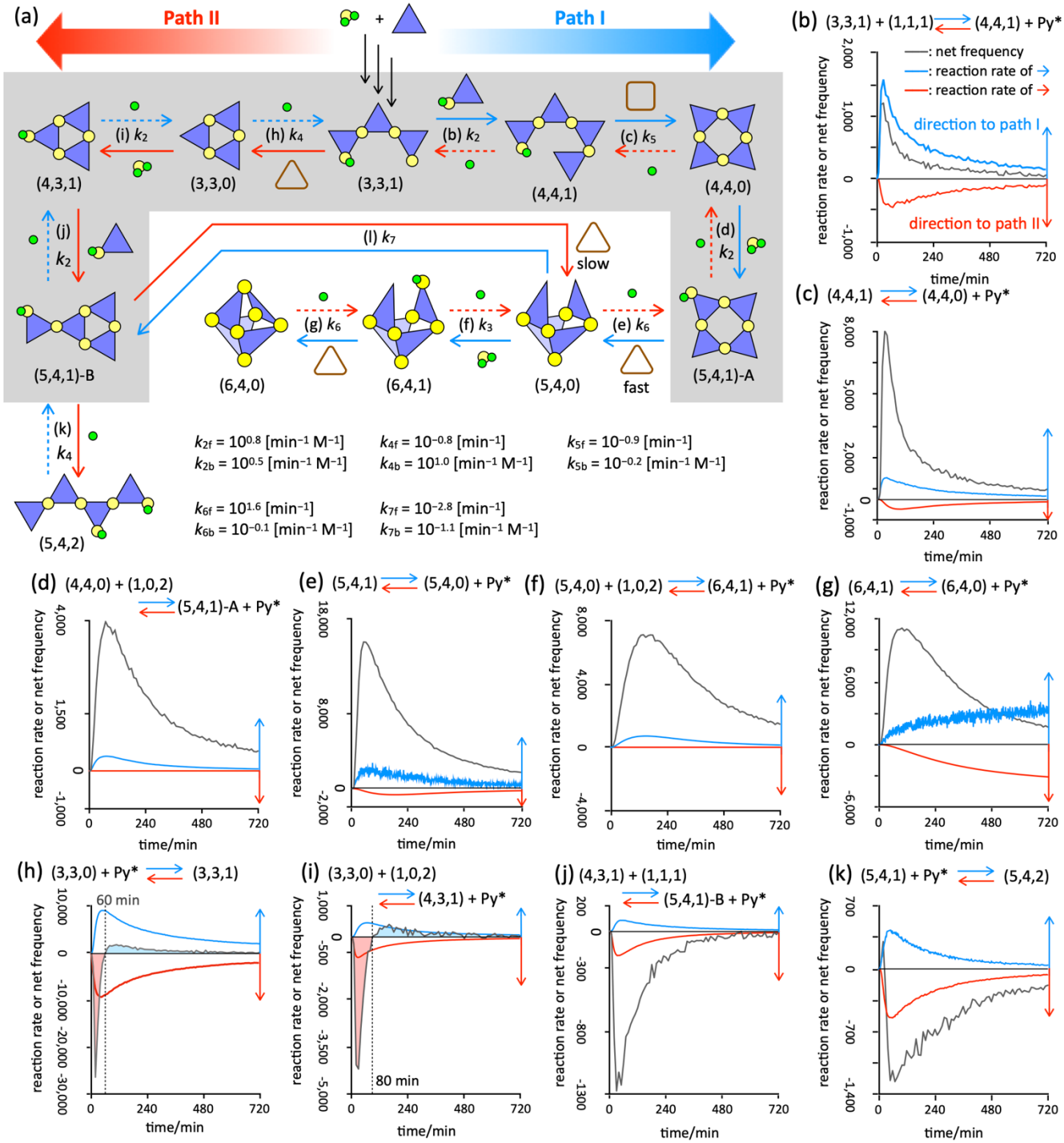

Figure 5. Reaction pathways through triangle and square formations to the $[\boldsymbol{Pd}_6\mathbf{1}_4]^{12+}$ truncated tetrahedron (TT). (a) A summary of the pathway selection in the self-assembly by the extended C-H principle. Reactions in a gray area correspond to a reversible reaction **A** ⇄ **B** in the model reaction networks in Fig. 2b and c, while (5,4,1)-A ⇄ (5,4,0) + Py* and (5,4,1)-B ⇄ (5,4,0) + Py* correspond to quasi-irreversible reactions **A** ⇄ **C** and **B** ⇄ **D**, respectively. (b)–(k) Net frequency and forward and backward reaction rates of the elementary reactions in (a). Alphabetic letters in the reaction arrows in (a) correspond to (b)–(k). Positive values indicate that the reaction proceeds in the blue arrow direction. Switching the direction of the reaction is emphasized by red and blue filled areas in (h) and (i). The reaction rate is the quantity defined in the Gillespie algorithm and directly related to the occurrence probabilities for the corresponding elementary reactions. The unit of the reaction rate is [min^{-1} × (number of molecules)] for both the first- (intramolecular) and the second-order (intermolecular) reactions. The time interval for counting the reaction frequency is increased as time proceed, to avoid the tiny fluctuations counted in shorter time intervals making the reaction directionality get blur.

In what follows, upon seeking of the extended concept of the C-H principle working in the self-assembly process of the $[\boldsymbol{Pd}_6\mathbf{1}_4]^{12+}$ TT, we elucidate (1) the main self-assembly pathway and (2) the dominant factors for the pathway selection focusing on the cyclization sequence (path **I** or **II**).

Main self-assembly pathway

The main self-assembly pathway linking the substrates and the $[\boldsymbol{Pd}_6\mathbf{1}_4]^{12+}$ TT, (6,4,0), was determined based on the reaction frequency analysis. The time evolution of the numbers (concentrations) of the species sometimes leads us to incorrect judgment of the species

rapidly converting to the next ones being considered as intermediate not participating in the major assembly pathways. The number of occurrences for each elementary reaction during the focused time region, that is, reaction frequency, is an appropriate parameter to find the major self-assembly pathways.[60] As the elementary reactions in the self-assembly are reversible, the direction of the reaction flow is determined by the difference between frequencies of the forward and the backward reactions (we call it the "net reaction frequency"). The main self-assembly pathway(s) can be found by connecting the elementary reactions with the high net reaction frequency (Table S1) from the product (the $[\boldsymbol{Pd}_6\mathbf{1}_4]^{12+}$ TT) to the substrates (**1** and $[\boldsymbol{Pd}\mathrm{Py}^*_2]^{2+}$). The main reaction pathway thus obtained (Fig. 4d) indicates that the self-assembly of the $[\boldsymbol{Pd}_6\mathbf{1}_4]^{12+}$ TT proceeds mainly through path **I** (square-triangle-triangle sequence).

Extended Curtin-Hammett principle in molecular self-assembly

The pathway selection in the molecular self-assembly can be interpreted by the extended C-H principle. Homology in pathway selection by the extended C-H principle was found between the model reaction networks (Fig. 2b and c) and the self-assembly of the $[\boldsymbol{Pd}_6\mathbf{1}_4]^{12+}$ TT (Fig. 5a). In the model reaction networks, the major pathway is determined by the quasi-irreversibility of **A** ⇄ **C** connected to a reversible reaction (**A** ⇄ **B**). In the self-assembly, a chain of elementary reactions (b), (c), (d), (h), (i), and (j) (a gray area in Fig. 5a) corresponds to **A** ⇄ **B** and the second bridging reactions, (e) and (l) in Fig 5a, correspond to **A** ⇄ **C** and **B** ⇄ **D** in the model networks, respectively.

The reaction rates and the net reaction frequencies of ten elementary reactions (b–k) in Fig. 5a are shown in Fig. 5b-k. The most important result is that emergence of quasi-irreversibility in intermolecular reactions in path **I**, (4,4,0) + (1,0,2) → (5,4,1)-A + Py* (Fig. 5d) and (5,4,0) + (1,0,2) → (6,4,1) + Py* (Fig. 5f), in spite of the rate constant k_{3b} being relatively large ($10^{0.4}$ $\mathrm{min^{-1}}$ $\mathrm{M^{-1}}$). It should be emphasized that though the same rate constants (k_{3f} and k_{3b}) are given in (3,3,0) + (1,0,2) ⇄ (4,3,1) + Py* in path **II** (Fig. 5i) a quasi-irreversible behavior was not observed. This contrasting behavior clearly indicates that the self-assembly pathway is not determined solely by the rate constants and that the reaction network structure is the key factor of pathway selection. The reason why (4,4,0) + (1,0,2) → (5,4,1)-A + Py* (Fig. 5d) and (5,4,0) + (1,0,2) → (6,4,1) + Py* (Fig. 5f) in path **I** are quasi-irreversible is because the products in these steps, (5,4,1)-A and (6,4,1), quickly convert into the next species, (5,4,0) and (6,4,0), by intramolecular bridging reactions, (5,4,1)-A → (5,4,0) + Py* (Fig. 5e) and (6,4,1) → (6,4,0) + Py* (Fig. 5g).

It is worth discussing why the oligomerization of (3,3,1) to give (4,4,1) followed by the square formation ((4,4,1) → (4,4,0) + Py*, Fig. 5c) is preferred to the triangle formation ((3,3,1) → (3,3,0) + Py*, Fig. 5h). Considering that generally intramolecular reactions are more advantageous than intermolecular ones at low concentration, under the experimental condition of the self-assembly of the $[\boldsymbol{Pd}_6\mathbf{1}_4]^{12+}$ TT ($[\mathbf{1}]_0$ = 2.0 mM), the triangle formation in path **II**, whose rate constant (k_{4f}) is $10^{-0.8}$ $\mathrm{min^{-1}}$, is expected to take place faster than the oligomerization (path **I**), whose rate constant (k_{2f}) is $10^{0.8}$ $\mathrm{min^{-1}}$ $\mathrm{M^{-1}}$ (k_{4f} > $k_{2f'}[\mathbf{1}]_0$). As expected, the cyclization of (3,3,1) to form (3,3,0) preferentially occurs until 60 min (a gray line with a red filled area in Fig. 5h). However, the reaction turns in the reverse direction after 60 min (a gray line with a blue filled area in Fig. 5h). A similar behavior was found in (3,3,0) + (1,0,2) ⇄ (4,3,1) + Py* in path **II** (Fig. 5i). As to the reactions in path **I**, the reverse of the reaction direction was not observed, and forward reactions (blue arrows in Fig. 5a) are always dominant (Fig. 5b-g). The switching of the direction of the reactions, (3,3,1) ⇄ (3,3,0) + Py* (Fig. 5h) and (3,3,0) + (1,0,2) ⇄ (4,3,1) + Py* (Fig. 5i) in path **II**, is caused by change in the concentrations of Py* and (3,3,1) during the self-assembly. The concentration of Py* increased with the reaction progress (Fig. 4a) and the concentration of (3,3,1) becomes low due to its conversion by the above mentioned quasi-irreversible steps. Consequently, the oligomerization of (3,3,1) to form (4,4,1) is preferred after 60 min *because of the emergence of quasi-irreversible steps in path **I***.

Conclusion

It was found from the numerical analysis of the reversible reaction networks that quasi-irreversibility appeared even though the constituent elementary reactions in the network are all reversible and that the quasi-irreversibility in reversible reaction networks is the origin of the pathway selection in molecular self-assembly. The quasi-irreversibility created in reversible reaction networks can be generally explained by extended concept of the Curtin-Hammett (C-H) principle, which was originally established for the fast conformational equilibrium with irreversible reactions.[64-67] Numerical facts on the pathway selection observed in a simple chain network model were found to be realized in a more realistic self-assembly system in which many first- (intramolecular) and second-order (intermolecular) elementary reactions are connected to the hub equilibrium reactions to construct a complicated network. In self-assembly systems, it is well known that sometimes kinetic traps can be obtained because of high energy barriers of their conversion.[37-41,68-70] However, their kinetic stability is not the only reason for their formation, and there should exist the reason why their formation process is selected. One of the answers to this question is the emergence of quasi-irreversible steps by the extended C-H principle. The rate constants, concentrations of substrates, products, and intermediate species, and the time evolution of and mutual relations among them are all related to the pathway selection. In other words, understanding the relationship among their factors based on the extended C-H principle make it possible to produce a desired metastable assembly or state in a rational way.

An emergence of quasi-irreversibility was achieved in a conceivably simplest reaction network model, where elementary first-order reactions are linked in series. This behavior is never totally reversible, while never be defined as exactly irreversible due to their individual reversible nature. A fine balance between the reversibility and the irreversibility can be considered as the superlative hybridization of them to generate what cannot be attained neither in a totally reversible nor in a totally irreversible system, and in essential part the Curtin-Hammett principle is found to function in its extended form.

Author contributions

S.H. conceived the project. S.T. established mathematical models and carried out all numerical simulation and analysis. S.H.., S.T.., and H.S. discussed numerical data. S.T. and S.H. prepared the manuscript, and all authors discussed the results and commented on the manuscript.

Conflicts of interest

There are no conflicts to declare.

Acknowledgements

This work was supported by JSPS KAKENHI grant numbers 19H02731, 19K22196, 20K05417, and 21K18974 and the Asahi Glass

Foundation. The authors thank Keisuke Takeuchi (The University of Tokyo) for his valuable comments on the manuscript.

References

1. Karlebach, G., and Shamir, R., Modelling and analysis of gene regulatory networks. *Nat. Rev. Mol. Cell Biol.*, **2008**, *9*, 770–780. DOI: 10.1038/nrm2503.
2. Ali Al-Radhawi, M., Del Vecchio, D., and Sontag, E. D., Multi-modality in gene regulatory networks with slow promoter kinetics. *PLoS Comput. Biol.*, **2019**, *15*, e1006784. DOI: 10.1371/journal.pcbi.1006784.
3. Barbuti, R., Roberta Gori, R., Milazzo, P., and Nasti, L., A survey of gene regulatory networks modelling methods: from differential equations to Boolean and qualitative bioinspired models. *J. Membr. Comput.*, **2020**, *2*, 207–226. DOI: 10.1007/s41965-020-00046-y.
4. Gerdts, C. J., Sharoyan, D. E., and Ismagilov, R. F., A Synthetic reaction network: Chemical amplification using nonequilibrium autocatalytic reactions coupled in time. *J. Am. Chem. Soc.*, **2004**, *126*, 6327–6331. DOI: 10.1021/ja031689l.
5. Kurylo, I., Gines, G., Rondelez, Y., Coffinier, Y., and Vlandas, A., Spatiotemporal control of DNA-based chemical reaction network via electrochemical activation in microfluidics. *Sci. Rep.*, **2018**, *8*, 6396. DOI: 10.1038/s41598-018-24659-7.
6. Novák, B., and Tyson, J., Design principles of biochemical oscillators. *Nat. Rev. Mol. Cell Biol.*, **2008**, *9*, 981–991. DOI: 10.1038/nrm2530.
7. Li, Z., and Yang, Q., Systems and synthetic biology approaches in understanding biological oscillators. *Quant. Biol.*, **2018**, *6*, 1-14. DOI: 10.1007/s40484-017-0120-7.
8. Tu, B., and McKnight, S., Metabolic cycles as an underlying basis of biological oscillations. *Nat. Rev. Mol. Cell Biol.*, **2006**, *7*, 696–701. DOI; 10.1038/nrm1980.
9. Friesen, W. O., Block, G. D., and Hocker, C. G., Formal approaches to understanding biological oscillators. *Annu. Rev. Physiol.*, **1993**, *55*, 661–681. DOI: 10.1146/annurev.ph.55.030193.003305.
10. Muñoz, J. J., Dingle, M., and Wenzel, M., Mechanical oscillations in biological tissues as a result of delayed rest-length changes. *Phys. Rev. E*, **2018**, *98*, 052409. DOI: 10.1103/PhysRevE.98.052409.
11. Helikar, T., Konvalina, J., Heidel, J., and Rogers, J. A., Emergent decision-making in biological signal transduction networks. *Proc. Nati. Acad. Sci. USA*, **2008**, *105*, 1913–1918. DOI: 10.1073/pnas.0705088105.
12. Bernabò, N., Barboni, B., and Maccarrone, M., The biological networks in studying cell signal transduction complexity: The examples of sperm capacitation and of endocannabinoid system. *Comput. and Struct. Biotech. J.*, **2014**, *11*, 11–21. DOI: 10.1016/j.csbj.2014.09.002.
13. Kestler, H. A., Wawra, C., Kracher, B., and Kühl, M., Network modeling of signal transduction: establishing the global view. *BioEssays.*, **2008**, *30*, 1037–1258. DOI: 10.1002/bies.20834.
14. Weng, G., Bhalla, U. S., and Iyengar, R., Complexity in biological signaling systems. *Science*, **1999**, *284*, 92–96. DOI: 10.1126/science.284.5411.92.
15. Bhalla, U. S., Understanding complex signaling networks through models and metaphors. *Prog. Biophys. Mol. Biol.*, **2003**, *81*, 45–65. DOI: 10.1016/S0079-6107(02)00046-9.
16. Eungdamrong, N J., and Iyengar, R., Modeling cell signaling networks. *Biol. Cell*, **2004**, *96*, 355–362. DOI: 10.1016/j.biolcel.2004.03.004.
17. Otero-Muras, I., Yordanov, P., and Stelling, J., Chemical reaction network theory elucidates sources of multistability in interferon signaling. *PLoS Comput. Biol.*, **2017**, *13*, e1005454. DOI: 10.1371/journal.pcbi.1005454.
18. Farquhar, G.D., von Caemmerer, S., and Berry, J. A., A biochemical model of photosynthetic CO_2 assimilation in leaves of C_3 species. *Planta*, **1980**, *149*, 78–90. DOI: 10.1007/BF00386231.
19. Pettersson, G., and Ryde-Pettersson, U., A mathematical model of the Calvin photosynthesis cycle. *Eur. J. Biochem.*, **1988**, *175*, 661–672. DOI: 10.1111/j.1432-1033.1988.tb14242.x.
20. Nelson, N., and Ben-Shem, A., The complex architecture of oxygenic photosynthesis. *Nat. Rev. Mol. Cell Biol.*, **2004**, *5*, 971–982. DOI: 10.1038/nrm1525.
21. Stirbet, A., Lazár, D., Guo, Y., and Govindjee, G., Photosynthesis: basics, history and modelling. *Annals of Botany*, **2020**, *126*, 511–537. DOI: 10.1093/aob/mcz171.
22. Jahan, N., Maeda, K., Matsuoka, Y., Sugimoto, Y., and Kurata, H., Development of an accurate kinetic model for the central carbon metabolism of *Escherichia coli*. *Microb. Cell Fact.*, **2016**, *15*, 112. DOI: 10.1186/s12934-016-0511-x.2.
23. Jeong, H., Tombor, B., Albert, R., Oltvai, Z. N., and Barabási, A.-L., The large-scale organization of metabolic networks. *Nature*, **2000**, *407*, 651–654. DOI: 10.1038/35036627.
24. Voit, E. O., The best models of metabolism. *WIREs Syst. Biol. Med.*, **2017**, *9*, e1391. DOI: 10.1002/wsbm.1391.
25. Costello, Z., and Martin, H. G., A machine learning approach to predict metabolic pathway dynamics from time-series multiomics data. *npj Syst. Biol. and Appl.*, **2018**, *4*, 19. DOI: 10.1038/s41540-018-0054-3.
26. Shen, F., Sun, R., Yao, J., Li, J., Liu, Q., Price, N. D., Liu, C., and Wang, Z., OptRAM: In-silico strain design via integrative regulatory-metabolic network modeling. *PLoS Comput. Biol.*, **2019**, *15*, e1006835. DOI: 10.1371/journal.pcbi.1006835.
27. Kurata, H., Virtual metabolic human dynamic model for pathological analysis and therapy design for diabetes. *iScience*, **2021**, *24*, 102101. DOI: 10.1016/j.isci.2021.102101.
28. Uematsu, S., Ohno, S., Tanaka, K. Y., Hatano, A., Kokaji, T., Ito, Y., Kubota, H., Hironaka, K.-i., Suzuki, Y., Matsumoto, M., et al., Multi-omics-based label-free metabolic flux inference reveals obesity-associated dysregulatory mechanisms in liver glucose metabolism. *iScience*, **2022**, *25*,103787. DOI: 10.1016/j.isci.2022.103787.
29. Feinberg, M., Chemical reaction network structure and the stability of complex isothermal reactors—I. The deficiency zero and deficiency one theorems. *Chem. Eng. Sci.*, **1987**, *42*, 2229–2268. DOI: 10.1016/0009-2509(87)80099-4.
30. Feinberg, M., Chemical reaction network structure and the stability of complex isothermal reactors—II. Multiple steady states for networks of deficiency one. *Chem. Eng. Sci.*, **1988**, *43*, 1–25. DOI: 10.1016/0009-2509(88)87122-7.
31. Robinson, W. E., Daines, E., van Duppen, P., de Jong, T., and Huck, W. T. S., Environmental conditions drive self-organization of reaction pathways in a prebiotic reaction network. *Nat. Chem.*, **2022**, *14*, 623–631. DOI: 10.1038/s41557-022-00956-7.
32. Huang, S., Li, F., Zhou, J. X., and Qian, H., Processes on the emergent landscapes of biochemical reaction networks and heterogeneous cell population dynamics: Differentiation in living matters. *J. R. Soc. Interface*, **2017**, *14*, 20170097. DOI: 10.1098/rsif.2017.0097.
33. van Roekel, H. W. H., Rosier, B. J. H. M., Meijer, L. H. H., Hilbers, P. A. J., Markvoort, A. J., Huck, W. T. S., and de Greef, T. F. A., Programmable chemical reaction networks: Emulating regulatory functions in living cells using a bottom-up approach. *Chem. Soc. Rev.*, **2015**, *44*, 7465–7483. DOI: 10.1039/C5CS00361J.
34. Barzel, B., and Barabási, A. L., Universality in network dynamics. *Nature Phys.*, **2013**, *9*, 673–681. DOI: 10.1038/nphys2741.
35. Fiedler, B., Mochizuki, A., Kurosawa, G., Saito, D., Dynamics and control at feedback vertex sets. I: Informative and determining nodes in regulatory networks. *J. Dyn. Diff. Equat.*, **2013**, *25*, 563–604. DOI: 10.1007/s10884-013-9312-7.
36. Mochizuki, A., Fiedler, B., Kurosawa, G., and Saito, D., Dynamics and control at feedback vertex sets. II: A faithful monitor to determine the diversity of molecular activities in regulatory networks. *J. Theor. Biol.*, **2013**, *335*, 130–146. DOI: 10.1016/j.jtbi.2013.06.009.

37. Varela, A. E., England, K. A., and Cavagnero, S., Kinetic trapping in protein folding, *Protein Eng. Des. Sel.*, **2019**, *32*, 103–108. DOI: 10.1093/protein/gzz018.
38. Mecha, M. F., Hutchinson, R. B., Lee, J. H., and Cavagnero, S., Protein folding in vitro and in the cell: From a solitary journey to a team effort. *Biophys. Chem.*, **2022**, *287*, 106821. DOI: 10.1016/j.bpc.2022.106821.
39. Suzuki, A., Aratsu, K., Datta, S., Shimizu, N., Takagi, H., Haruki, R., Adachi, S., Hollamby, M., Silly, F., and Yagai, S., Topological impact on the kinetic stability of supramolecular polymers. *J. Am. Chem. Soc.*, **2019**, *141*, 13196−13202. DOI: 10.1021/jacs.9b06029.
40. Yoneya, M., Tsuzuki, S., Yamaguchi, T., Sato, S., and Fujita, M., Coordination-directed self-assembly of $M_{12}L_{24}$ nanocage: Effects of kinetic trapping on the assembly process. *ACS Nano*, **2014**, 8, 1290−1296. DOI: 10.1021/nn404595j.
41. Hagan, M. F., Elrad, O. M., and Jack, R. L., Mechanisms of kinetic trapping in self- assembly and phase transformation. *J. Chem. Phys.*, **2011**, *135*, 104115. DOI: 10.1063/1.3635775.
42. Gold, V., Glossary of terms used in physical organic chemistry. *Pure Appl. Chem.*, **1979**, *51*, 1725–1801. DOI: 10.1351/pac197951081725.
43. Seeman, J. I., Sanders, E. B., and Farone, W. A., Uses and analyses of Curtin-Hammett/Winstein-Holness systems involving second order reactions. *Tetrahedron*, **1980**, *36*, 1173–1177. DOI: 10.1016/0040-4020(80)87014-1.
44. Seeman, J. I., Effect of conformational change on reactivity in organic chemistry. Evaluations, applications, and extensions of Curtin-Hammett/Winstein-Holness kinetics. *Chem. Rev.*, **1983**, *83*, 83-142. DOI: 10.1021/cr00054a001.
45. Seeman, J. I., The Curtin-Hammett principle and the Winstein-Holness equation: new definition and recent extensions to classical concepts. *J. Chem. Educ.*, **1986**, *63*, 42. DOI: 10.1021/ed063p42.
46. Chakraborty, S., and Saha, C., The Curtin-Hammett principle. *Resonance*, **2016**, *21*, 151–171. DOI: 10.1007/s12045-016-0307-7.
47. Gillespie, D. T., A general method for numerically simulating the stochastic time evolution of coupled chemical reactions. *J. Comput. Phys.*, **1976**, *22*, 403–434. DOI: 10.1016/0021-9991(76)90041-3.
48. Gillespie, D. T., Exact stochastic simulation of coupled chemical reactions. *J. Phys. Chem.*, **1977**, *81*, 2340–2361. DOI: 10.1021/j100540a008.
49. Gillespie, D. T., A rigorous derivation of the chemical master equation. *Physica A Stat. Mech. its Appl.*, **1992**, *188*, 404–425. DOI: 10.1016/0378-4371(92)90283-V.
50. Gillespie, D. T., Stochastic simulation of chemical kinetics. *Annu. Rev. Phys. Chem.*, **2007**, *58*, 35–55. DOI: 10.1146/annurev.physchem.58.032806.104637.
51. Fujita, M., Oguro, D., Miyazawa, M., Oka, H., Yamaguchi, K., and Ogura, K., Self-assembly of ten molecules into nanometre-sized organic host frameworks. *Nature*, **1995**, *378*, 469–471. DOI: 10.1038/378469a0.
52. Baba, A., Kojima, T., and Hiraoka, S., Self-assembly process of dodecanuclear Pt(II)-linked cyclic hexagon. *J. Am. Chem. Soc.*, **2015**, *137*, 7664–7667. DOI: 10.1021/jacs.5b04852.
53. Tsujimoto, Y., Kojima, T., and Hiraoka, S., Rate-determining step in the self-assembly process of supramolecular coordination capsules. *Chem. Sci.*, **2014**, *5*, 4167–4172. DOI: 10.1039/C4SC01652A.
54. Kai, S., Sakuma, Y., Mashiko, T., Kojima, T., Tachikawa, M., and Hiraoka, S., The effect of solvent and coordination environment of metal source on the self-assembly pathway of a Pd(II)-mediated coordination capsule. *Inorg. Chem.*, **2017**, *56*, 12652–12663. DOI: 10.1021/acs.inorgchem.7b02152.
55. Hiraoka, S., What do we learn from the molecular self-assembly process? *Chem. Rec.*, **2015**, *15*, 1144–1147. DOI: 10.1002/tcr.201510005.
56. Hiraoka, S., Unresolved issues that remain in molecular self-assembly. *Bull. Chem. Soc. Jpn.*, **2018**, *91*, 957–978. DOI: 10.1246/bcsj.20180008.
57. Hiraoka, S., Self-assembly processes of Pd(II)- and Pt(II)-linked discrete self-assemblies revealed by QASAP. *Isr. J. Chem.*, **2019**, *59*, 151–165. DOI: 10.1002/ijch.201800073.
58. Matsumura, Y., Hiraoka, S., and Sato, H., A reaction model on the self-assembly process of octahedron-shaped coordination capsules. *Phys. Chem. Chem. Phys.*, **2017**, *19*, 20338–20342. DOI: 10.1039/c7cp03493h.
59. Takahashi, S., Sasaki, Y., Hiraoka, S., and Sato, H., A stochastic model study on the self-assembly process of a Pd_2L_4 cage consisting of rigid ditopic ligands. *Phys. Chem. Chem. Phys.*, **2019**, *21*, 6341–6347. DOI: 10.1039/C8CP06102E.
60. Takahashi, S., Tateishi, T., Sasaki, Y., Sato, H., and Hiraoka S., Towards kinetic control of coordination self-assembly: A case study of a Pd_3L_6 double-walled triangle to predict the outcomes by a reaction network model. *Phys. Chem. Chem. Phys.*, **2020**, *22*, 26614–26626. DOI: 10.1039/d0cp04623j.
61. Komine, S., Takahashi, S., Kojima, T., Sato, and H., Hiraoka, S., Self-assembly processes of octahedron-shaped Pd_6L_4 cages. *J. Am. Chem. Soc.*, **2019**, 141, 3178–3186. DOI: 10.1021/jacs.8b12890.
62. Zhang, X., Takahashi, S., Aratsu, K., Kikuchi, I., Sato, H., and Hiraoka, S., Cyclization or bridging: Which occurs faster is the key to the self-assembly mechanism of Pd_6L_3coordination prisms. *Phys. Chem. Chem. Phys.*, **2022**, *24*, 2997–3006. DOI: 10.1039/D1CP04448F.
63. Hiraoka, S., Takahashi, S., and Sato, H., Coordination self-assembly processes revealed by collaboration of experiment and theory: toward kinetic control of molecular self-assembly. *Chem. Rec.*, **2021**, *21*, 443–459. DOI: 10.1002/tcr.202000124.
64. Barton, D. H. R., The conformation of the steroid nucleus. *Experientia*, **1950**, *6*, 316–320. DOI: 10.1007/BF02170915.
65. Barton, D. H. R., The stereochemistry of cyclohexane derivatives. *J. Chem. Soc.*, **1953**, 1027–1040. DOI: 10.1039/JR9530001027.
66. Pollak, P. I., and Curtin, D. Y., Stereospecificity in the rearrangement of amino alcohols. *J. Am. Chem. Soc.*, **1950**, *72*, 961–965. DOI: 10.1021/ja01158a082.
67. Curtin, D. Y., and Crew, M. C., Rearrangement with nitrous acid of the diastereoisomeric 1-p-anisyl-1-phenyl-2-aminopropanols. The *cis* effect of methyl and phenyl groups[1]. *J. Am. Chem. Soc.*, **1955**, *77*, 354–357. DOI: 10.1021/ja01607a034.
68. Shin, S.-H., Chung, S., Sanii, B., Comolli, L. R., Bertozzi, C. R., and De Yoreo, J. J., Direct observation of kinetic traps associated with structural transformations leading to multiple pathways of S-layer assembly. *Proc. Nati. Acad. Sci. USA*, **2012**, *109*, 12968–12973. DOI: 10.1073/pnas.1201504109.
69. Treiber, D. K., and Williamson, J. R., Exposing the kinetic traps in RNA folding. *Curr. Opin. Struct. Biol.*, **1999**, *9*, 339−345. DOI: 10.1016/S0959-440X(99)80045-1.
70. Yan, Y., Huang, J., and Tang, B. Z., Kinetic trapping– Strategy for directing the self-assembly of unique functional nanostructures. *Chem. Commun.,* **2016**, *52*, 11870–11884. DOI: 10.1039/C6CC03620A.